CrossMark

ORIGINAL PAPER

Modeling and estimation of production rate for the production phase of non-growth-associated high cell density processes

Martín Jamilis[1] · **Fabricio Garelli**[1] · **Md Salatul Islam Mozumder**[2,3] ·
Teresita Castañeda[4] · **Hernán De Battista**[1]

Abstract This paper addresses the estimation of the specific production rate of intracellular products and the modeling of the bioreactor volume dynamics in high cell density fed-batch reactors. In particular, a new model for the bioreactor volume is proposed, suitable to be used in high cell density cultures where large amounts of intracellular products are stored. Based on the proposed volume model, two forms of a high-order sliding mode observer are proposed. Each form corresponds to the cases with residual biomass concentration or volume measurement, respectively. The observers achieve finite time convergence and robustness to process uncertainties as the kinetic model is not required. Stability proofs for the proposed observer are given. The observer algorithm is assessed numerically and experimentally.

✉ Martín Jamilis
   martin.jamilis@ing.unlp.edu.ar

1   Group of Control Applications, LEICI, Faculty of
    Engineering, La Plata National University, CONICET,
    C.C.91 (1900), La Plata, Argentina

2   Department of Biosystems Engineering, Ghent University,
    Coupure Links 653, 9000 Ghent, Belgium

3   Business Unit Separation and Conversion Technology,
    Flemish Institute for Technological Research (VITO),
    Boeretang 200, 2400 Mol, Belgium

4   Research and Development Center for Industrial
    Fermentations (CINDEFI), School of Science, La Plata
    National University, CONICET, 47 and 115,
    B1900ASH La Plata, Argentina

Introduction

High cell density (HCD) processes constitute a class of bioprocesses with many obstacles for the direct application of standard control and estimation solutions. To begin with, sensing variables in the bioreactor is more difficult than in other process: the use of online optical density is nearly impossible because of the opacity of the media. In many cases, the amount of foam is excessive, which troubles standard-level measurements used to compute the volume. Also, substrate measurements are difficult in many waste treatment processes, due to its variable composition and impurities. Another issue present in HCD processes is that the volumes of both the biotic and abiotic phases are significant to the overall volume, especially if an intracellular product is being produced. In these cases, integrating media culture flow rates ceases to be an accurate method to estimate the bioreactor volume. Better models are needed to estimate the culture volume taking into account the volume of the living components.

Bioprocesses for waste treatment and removal are well-known high cell density processes. Moreover, many kinds of fermentations can be performed to obtain high added value products from residues mainly produced by the industry, such as glycerol, sugarcane mash and wastewater. For example, *Polyhydroxybutyrate* (PHB) is a biodegradable polymer suitable for thermoprocessing applications [21] that can be obtained from different carbon sources such as glycerol coming from biodiesel industry, using for instance the bacteria *Cupriavidus necator* [15, 16]. PHB is an intracellular product and can be produced mainly in a non-growth-associated manner and reach levels of 90 % of cell dry weight [21]. The non-growth-associated process has two phases; in the growth phase, a vast quantity of cells is produced while hardly any PHB is generated due to

unfavorable medium conditions. In the production phase, PHB generation is stimulated by stopping cell proliferation and letting the nitrogen source deplete completely. To obtain great quantities of product in short times, a high cell concentration needs to be achieved in the growth phase. Another example of HCD process is lipid production to be later used for biodiesel production by transesterification. Research has been done on the use of microalgae and yeasts such as *Rhodosporidium toruloides* to produce lipids [11, 18, 26], as before, high productivities require large cell concentrations, and the production of the lipid can be done in a non-growth-associated manner. These HCD processes and others share some common characteristics like non-growth-associated intracellular product storage and large product to biomass ratios (large biotic volume). Also, high productivities are always pursued. More examples of high cell density processes are covered in [22].

As mentioned above, one of the main obstacles met when using wastes as substrate for fermentations is the presence of impurities combined with composition variability and uncertainty. For this reason, standard control methods like exponential feeding may become ineffective and far from optimal. In cases where the microorganism growth or productivity is inhibited by the excess of some substrate (Haldane like kinetics), suboptimal operation and even instabilities can show up [2]. A method to solve this shortcoming is the implementation of closed-loop controllers to feed the reactor depending on the actual state of the process. For example, if the objective was to maximize the productivity of a certain product or to keep a given production rate, the ideal solution would be to define the substrate feeding rate based on the production rate (feedback control or closed loop control). The same concept applies for growth rate regulation [3, 5]. The process rates hold important information about the process state; their knowledge is not only important for control but also for monitoring, i.e., fault detection, physiological studies and operating point verification. The most important restriction regarding closed-loop process control and monitoring is that growth and production rates cannot be measured directly by any sensor. Moreover, their determination from the measurement of any process concentration involves differentiation with respect to time which typically amplifies the measurement noise.

The lack of reaction rate measurement can be overcome with software sensors. In this field, state observers allow estimating unknown variables of the process with an error decreasing with time, using previous knowledge of the process behavior (a model), inputs and measured outputs. Depending on the case, exponential and asymptotic observers are the most widespread structures [6, 8]. One of the main characteristics of these observers is the asymptotic convergence of the error. In the case of the asymptotic observers, the response is often slow and cannot be tuned by design; thus a good initial estimate is needed. In the exponential case, the speed can be adjusted by design; however, high speeds may lead to bad noise or perturbation rejection. Another issue present in these observers is that variations in the estimated rate appear as perturbations that cannot be rejected, i.e., the error converges to a bounded neighborhood around zero. Another class of observer are the sliding-mode (SM) observers, where a discontinuous signal is used as a correction term for the model prediction. These observers do not introduce additional dynamics to the estimation and have a better performance with regard to convergence speed and disturbance rejection than the exponential ones. Also, the convergence is obtained in finite time, which is important because the processes usually have a limited duration. A distinction can be made between the first- and high-order SM observers. Both share the previous advantages with the difference that when used for growth or production rate estimation, the estimated rate obtained by the first-order observer is discontinuous. Then, it is necessary to filter it and additional dynamics are nevertheless introduced [20]. High-order SM observers are more advanced algorithms and allow obtaining a continuous estimation for the growth and production rates [4, 17, 25]. An important strength of these observers is that there is no tracking error against bounded changes in the variable being estimated.

The construction of proper estimation algorithms for HCD processes is complicated by the lack of proper volume models. Common practices like integrating the flow rate to obtain the accumulated volume are invalid in this case. Early proposals like [24] suggest that cell volume should be accounted in HCD processes for broth volume calculation. In [23], biomass estimations and a volume model are proposed making use of gas analysis equipment and a uniform density of the bioreactor broth is assumed. In [7], biomass concentration estimations are also made by means of dielectric spectroscopy and gas analysis. In [8], a switched observer scheme is proposed for growth rate estimation in high cell density PHB production processes addressing biomass measurement issues.

In this article, a dynamical model for the bioreactor volume in HCD processes is proposed, which accounts for the volume of the cells and product in the bioreactor and the densities of the liquids being mixed. Then, a high-order sliding mode (HOSM) observer is proposed to estimate the production rate in HCD processes exploiting the information given by the volume changes in the bioreactor. First, in Sect. 2, a model is proposed for the volume variations in relation to the production rate. Then, two versions of an HOSM observer are proposed in Sect. 3 to estimate the production rate along with stability proofs. Simulation and experimental results are shown in Sect. 4.

Model development

Process model under unbalanced feeding

Unbalanced feeding conditions are used in many processes to boost the production of a given product. For example, PHB production using the bacteria *C. necator* is enhanced under nitrogen starvation conditions that results in no growth at all [15, 16]. The same technique has been used in lipids production for second-generation biodiesel industry; with yeast such as *Rhodosporidium toruloides*, nitrogen starvation boosts production and again prevents growth [11, 18, 26]. Keeping these examples in mind, the process model can be stated for the cases where unbalanced feeding is used during the production stages. Then, for the next steps, it is considered that nitrogen starvation is used to enhance production and that as a result there is no growth. In this work, residual biomass is defined as the fraction of total biomass that is not the product, namely cell structure, organelles and cytoplasm. If nitrogen starvation is applied and there is no growth, the amount of residual biomass remains constant for the rest of the process:

Assumption 1 $\dot{X} = 0$ and $X = X(t_0)$ is a known constant.

The simplified chemical reaction is:

$$s \rightarrow y_{ps}p$$
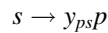
and the dynamical model for this condition in terms of the total masses of residual biomass, carbon source and product is[1]:

$$\dot{X} = 0 \tag{1}$$

$$\dot{P} = \mu_{ps}X \tag{2}$$

$$\dot{S} = -\frac{\mu_{ps}X}{y_{ps}} + F_s s_f, \tag{3}$$

where uppercase X, S and P are the total masses of residual biomass, carbon source and product in the bioreactor, μ_{ps} is the non-growth-associated production rate, y_{ps} is the carbon source to product yield, F_s is the feeding flow rate and s_f is the carbon source concentration in the media reservoir.

Volume model

In this section, a novel approach is proposed for modeling the bioreactor volume dynamics in high cell density fed-batch processes. It is considered that in the process, a carbon substrate is fed to the bioreactor to produce residual biomass and an intracellular product. The volume

variations are considered as the result of the contribution of three separate sources, the addition of substrate medium to the bioreactor, the substrate consumption and the accumulation of the product. Finally, a simplified model is obtained under the assumption that carbon source concentration is kept constant with an appropriate control. The simplest model for the volume dynamics of a fed-batch process states that the volume change is equal to the flow rate of liquids pumped into the bioreactor:

$$\dot{V} = F. \tag{4}$$

Although this model is accurate enough for many applications, it is inexact for the cases studied in this work, mainly because of the high cell density and the large amounts of intracellular product. To begin with, the density of the product is not equal to the density of the substrate consumed for its production. Moreover, the fed substrate is consumed quickly by the vast amount of cells; thus, it may be fed at a concentration s_f much higher than the desired concentration s_r inside the bioreactor to avoid large volume changes or dilutions. This introduces another density change between the fed media and the bioreactor media. Secondly, since a large amount of intracellular product is stored, the size of the cells must increase accordingly. For example, it has been shown that *C. necator* increases its volume proportionally to the intracellular PHB content [19]. Hence, the volume of the cells may affect the volume changes of the process. Then, as the product is contained inside the cells and is not dissolved in the medium, the total volume is the sum of the medium volume V_m and the cells volume V_c:

$$V = V_m + V_c, \tag{5}$$

and differentiates with respect to time

$$\dot{V} = \dot{V}_m + \dot{V}_c. \tag{6}$$

Since there is no cell proliferation, the change in the cell volume is equal to the change in the product volume V_p, which can be obtained as

$$\dot{V}_c = \dot{V}_p = \frac{\dot{P}}{\rho_p}, \tag{7}$$

where ρ_p is the product density. Then, replacing (2) in (7),

$$\dot{V}_p = \frac{\mu_{ps}X}{\rho_p}. \tag{8}$$

This term is significant as long as the quantities of product stored in the cells are large and comparable to the medium volume change $\dot{V}_m$.

The second term of (6) is the medium volume change, which can be obtained from the mass balance in (3). Defining the carbon source concentration as the total carbon source mass over the medium volume

---

[1] The dot operator · indicates time differentiation.

$$s = \frac{S}{V_m} \tag{9}$$

$$\Rightarrow \dot{S} = \dot{s}V_m + s\dot{V}_m \tag{10}$$

and replacing (10) in (3),

$$\dot{s}V_m + s\dot{V}_m = -\frac{\mu_{ps}X}{y_{ps}} + F_s s_f \tag{11}$$

$$\Rightarrow \dot{V}_m = -\frac{\mu_{ps}X}{s y_{ps}} + F_s \frac{s_f}{s} - V_m \frac{\dot{s}}{s}. \tag{12}$$

Then, assuming that the carbon source concentration in the media is being adequately regulated at a constant value, the last term of (12) can be neglected, because $\dot{s} = 0$ and the carbon source concentration is constant and equal to the reference value $s = s_r$:

$$\dot{V}_m = -\frac{\mu_{ps}X}{s_r y_{ps}} + F_s \frac{s_f}{s_r}. \tag{13}$$

Finally, the volume dynamic model is obtained by replacing (8) and (13) in (6)

$$\dot{V} = F_s \frac{s_f}{s_r} - \frac{\mu_{ps}X}{s_r y_{ps}} + \frac{\mu_{ps}X}{\rho_p}, \tag{14}$$

where all the parameters involved are referenced in Table 1. It can be noticed that the volume model (14) accounts for the contribution of the media flow rate, the carbon source consumption and the product formation (first, second and third terms, respectively).

The following constants are defined:

$$\gamma = \frac{s_f}{s_r} \tag{15}$$

$$v = -\frac{1}{s_r y_{ps}} + \frac{1}{\rho_p}. \tag{16}$$

Then, the model (14) reduces to:

$$\dot{V} = F_s \gamma + \mu_{ps} v X. \tag{17}$$

Remark 1 It is possible to obtain a model with the same structure as (14) and (17) by calculating the volume of the media in the bioreactor using the partial molar volumes of water and the carbon source being used. This approach is equally valid, but requires the knowledge of more parameters (densities and partial molar volumes). The assumption that carbon source concentration is constant is also necessary, since partial molar volumes are functions of that concentration.

Model reduction

As the total residual biomass X is constant and known throughout the production phase, it is convenient to

Table 1 Model parameters

Name	Description	Units
X	Residual biomass mass	(g)
S	Carbon source mass	(g)
P	Product mass	(g)
x	Residual biomass concentration	(g/l)
s	Carbon source concentration	(g/l)
p	Product concentration	(g/l)
F_s	Carbon source flow rate	(l/h)
s_f	Carbon source concentration in the reservoir	(g/l)
s_r	Carbon source concentration regulated by control	(g/l)
ρ_p	Density of the product	(g/l)
μ_{ps}	Specific production rate	(1/h)
y_{ps}	Carbon source to product yield	(g/g)
V	Volume of the bioreactor content	(l)
V_m	Volume of media in the bioreactor	(l)
V_c	Volume occupied by cells	(l)
V_p	Volume occupied by product	(l)
D	Dilution rate	(1/h)
γ	Parameter of the proposed volume model	
v	Parameter of the proposed volume model	(l/g)
$\hat{x}$	Estimated residual biomass concentration	(g/l)
$\hat{\mu}_{ps}$	Estimated specific production rate	(1/h)
σ	Proposed sliding function	
$\tilde{x}$	Residual biomass concentration estimation error	(g/l)
$\tilde{\mu}_{ps}$	Specific production rate estimation error	(1/h)
α	Gain of the proposed observers	
β	Gain of the proposed observers	
$\bar{\rho}$	Bound for $\dot{\mu}_{ps}$	
f_{phb}	Intracellular PHB content ratio (Sect. 4)	(g/g)

redefine the volume in terms of residual biomass concentration or conversely depending on which one is measured online. This reduces the number of variables in the model and makes the observer formulation easier. The residual biomass concentration is defined as:

$$x = X/V. \tag{18}$$

Then, differentiating (18) and replacing (1),

$$\dot{x} = -Dx \tag{19}$$

$$D = \dot{V}/V. \tag{20}$$

Note that although the dilution rate D is usually defined as the quotient of the flow rate over the volume, in this work a more general definition (20) has been used.

Carbon source and product concentrations can be obtained in the same way. The concentrations are defined as

$$p = \frac{P}{V} \tag{21}$$

$$s = \frac{S}{V_m}, \tag{22}$$

and differentiating with respect to time

$$\dot{p} = \mu_{ps}x - Dp \tag{23}$$

$$\dot{s} = -\frac{\mu_{ps}X}{y_{ps}V_m} - \frac{\dot{V}_m}{V_m}s + \frac{F_s}{V_m}s_f. \tag{24}$$

Finally, in the case that residual biomass concentration x is measured, the volume and dilution are determined as

$$V = \frac{X}{x} \tag{25}$$

$$D = \frac{F_s\gamma x}{X} + \mu_{ps}xv, \tag{26}$$

which replaced in (19) give the residual biomass model:

$$\dot{x} = -\left(\frac{F_s\gamma}{X} + \mu_{ps}v\right)x^2. \tag{27}$$

In the scenario in which volume is the measured variable, biomass concentration can be determined as in (18) and the volume model is the one given in (17):

$$x = \frac{X}{V} \tag{28}$$

$$\dot{V} = F_s\gamma + \mu_{ps}vX. \tag{29}$$

From these equations, the production rate observer can be designed for each case.

Proposed observer

In this section, an HOSM observer is proposed to estimate the specific production rate of the process. The proposed observer is a reformulation of the super-twisting algorithm [9] to account for the specific nonlinearities of the process under study.

The observer is presented in two different forms depending on which variable is measured online, residual biomass or volume. The following assumptions are made:

Assumption 2 The coefficients v and γ are known.

Assumption 3 The production rate derivative can be bounded: $|\dot{\mu}_{ps}| < \bar{\rho}$.

The first assumption depends on the modeling of the process and knowledge of the densities and concentrations; however, some errors are admissible and stability is never compromised. The second assumption states that the

kinetic model is unnecessary for the observer, and it is only required to know a bound of how fast the rate can change.

Observer for the case with residual biomass measurement

The first form of the observer is for the scenario in which residual biomass concentration can be measured independently of the accumulated product; see for instance [10, 13].

First, Eq. (27) is rewritten as:

$$\dot{x} = \left(-v\mu_{ps} + f(x,t)\right)x^2, \tag{30}$$

where $f(x,t) = -\frac{F_s\gamma}{X}$ is a function of the input.

The proposed observer equations are:

$$\begin{cases} \dot{\hat{x}} &= \left(-v\hat{\mu}_{ps} + f(x,t) - (\bar{\rho}v)2\beta|\sigma|^{\frac{1}{2}}\operatorname{sign}(\sigma)\right)\hat{x}^2 \\ \dot{\hat{\mu}}_{ps} &= \bar{\rho}\alpha\operatorname{sign}(\sigma) \\ \sigma &= (\bar{\rho}v)^{-1}(x^{-1} - \hat{x}^{-1}), \end{cases} \tag{31}$$

where $\hat{x}$ and $\hat{\mu}_{ps}$ are the estimated residual biomass and production rate, respectively, α and β are design gains, $\bar{\rho}$ is the bound for the production rate derivative and σ is the sliding function. Usually, the sliding function is defined as the estimation error in the measured variable $x - \hat{x}$; however, in this work a different function is proposed to account for the particular nonlinearities of the process and ensure the stability of the estimate.

Stability analysis

The stability proof for this observer is performed in two steps. First, a polytopic linear differential inclusion (PLDI) that covers all the possible error trajectories is defined. Second, the stability of the PLDI is obtained in the sense of Lyapunov for a set of gains α and β.

The estimation errors are defined as $\tilde{x} = x - \hat{x}$ and $\tilde{\mu}_{ps} = \mu_{ps} - \hat{\mu}_{ps}$; then by differentiation and replacing (27), (31) the error equations are obtained:

$$\dot{\tilde{x}} = -v(\mu x^2 - \hat{\mu}\hat{x}^2) - f(x,t)(x^2 - \hat{x}^2) + (\bar{\rho}v\hat{x}^2)2\beta|\sigma|^{\frac{1}{2}}\operatorname{sign}(\sigma). \tag{32}$$

$$\dot{\tilde{\mu}}_{ps} = \dot{\mu}_{ps} - \bar{\rho}\alpha\operatorname{sign}(\sigma). \tag{33}$$

Proposition 1 *If the change of coordinates*

$$\xi = \begin{bmatrix} \bar{\rho}|\sigma|^{\frac{1}{2}}\operatorname{sign}(\sigma) \\ \tilde{\mu}_{ps} \end{bmatrix} \tag{34}$$

is applied to Eqs.(32) and (33), it can be concluded that

$$\dot{\xi} = \frac{\bar{\rho}}{|\xi_1|}A(t)\xi \quad A(t) \in \mathcal{A}, \tag{35}$$

where $\mathcal{A}$ is a polytopic linear differential inclusion (PLDI):

$$\begin{aligned}
\mathcal{A} &= \mathrm{conv}(A_1, A_2) \\
A_1 &= \begin{bmatrix} -\beta & 1/2 \\ -\alpha + 1 & 0 \end{bmatrix}. \\
A_2 &= \begin{bmatrix} -\beta & 1/2 \\ -\alpha - 1 & 0 \end{bmatrix}
\end{aligned} \tag{36}$$

Proof First, from Eq. (34), ξ_1 is differentiated:

$$\dot{\xi}_1 = \bar{\rho}\left(\frac{1}{2}|\sigma|^{-\frac{1}{2}}\mathrm{sign}(\sigma)\dot{\sigma}\,\mathrm{sign}(\sigma) + 0\right) = \frac{\bar{\rho}}{2|\sigma|^{\frac{1}{2}}}(\dot{\sigma}).$$

Next, by differentiating σ in (31) and replacing:

$$\dot{\xi}_1 = \frac{\bar{\rho}}{2|\sigma|^{\frac{1}{2}}}\left(\frac{\tilde{\mu}}{\bar{\rho}} - 2\beta|\sigma|^{\frac{1}{2}}\mathrm{sign}(\sigma)\right) = \frac{1}{|\sigma|^{\frac{1}{2}}}\left(\frac{\tilde{\mu}}{2} - \beta\xi_1\right).$$

Then, by replacing $|\xi_1| = \bar{\rho}|\sigma|^{\frac{1}{2}}$:

$$\dot{\xi}_1 = \frac{\bar{\rho}}{|\xi_1|}\left(\frac{\tilde{\mu}}{2} - \beta\xi_1\right).$$

Second, ξ_2 from Eq. (34) is differentiated:

$$\dot{\xi}_2 = \dot{\mu} - \bar{\rho}\alpha\,\mathrm{sign}(\sigma) = \bar{\rho}\,\mathrm{sign}(\sigma)\left(\frac{\dot{\mu}}{\bar{\rho}\,\mathrm{sign}(\sigma)} - \alpha\right).$$

Since $\bar{\rho}$ is the bound for $\dot{\mu}_{ps}$, the first term in the parenthesis can be replaced by a parameter $U \in [-1, 1]$:

$$\dot{\xi}_2 = \frac{\xi_1}{|\sigma|^{\frac{1}{2}}}(U - \alpha) = \frac{\bar{\rho}}{|\xi_1|}(U - \alpha)\xi_1.$$

Finally, the following system is obtained:

$$\dot{\xi} = \frac{\bar{\rho}}{|\xi_1|}\begin{bmatrix} -\beta & 1/2 \\ U - \alpha & 0 \end{bmatrix}\xi.$$

$\square$

A PLDI is said to be quadratic stable if there exists a Lyapunov quadratic function $V(\xi) = \xi^T P\xi$, $P \succ 0$ that decreases along every nonzero trajectory [1], i.e., $\dot{V}(\xi) < 0$. A necessary and sufficient condition for that is

$$P \succ 0, \quad A_i^T P + PA_i \prec 0 \quad \forall i = 1, 2, \tag{37}$$

which is verified in:

$$\dot{V}(\xi) = \frac{\bar{\rho}}{|\xi_1|}\xi^T\left(A(t)^T P + PA(t)\right)\xi < 0. \tag{38}$$

Note that $\frac{\bar{\rho}}{|\xi_1|}$ is positive, then the Lyapunov function will decrease as long as (37) holds.

The problem can be translated into a generalized eigenvalue problem [1] by rewriting the PLDI matrices:

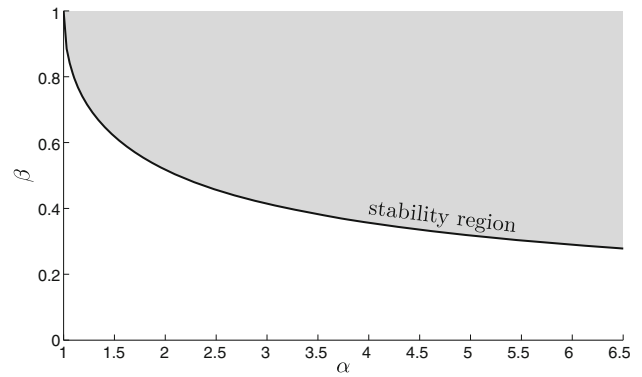$$A_1 = \beta A_0 + A_1', \tag{39}$$

$$A_2 = \beta A_0 + A_2', \tag{40}$$

Fig. 1 Set of stable gains α and β

$$\begin{aligned}
A_0 &= \begin{bmatrix} -1 & 0 \\ 0 & 0 \end{bmatrix} \\
A_1' &= \begin{bmatrix} 0 & 1/2 \\ (1 - \alpha) & 0 \end{bmatrix} \quad A_2' = \begin{bmatrix} 0 & 1/2 \\ (-1 - \alpha) & 0 \end{bmatrix}.
\end{aligned} \tag{41}$$

Then, for different values of $\alpha > 1$, the objective is to search for the minimum β gain for which quadratic stability is achieved:

$$\begin{cases} P \succ 0 \\ (A_1'^T P + PA_1') + \beta(A_0^T P + PA_0) \prec 0 \\ (A_2'^T P + PA_2') + \beta(A_0^T P + PA_0) \prec 0. \end{cases} \tag{42}$$

Problem (42) is quasi-convex and can be solved by applying bisection on β and checking the feasibility of the problem for every iteration. The numerical computations were done with YALMIP software [12]. Figure 1 plots the (α, β) pairs for which quadratic stability is guaranteed.

Remark 2 If the carbon source concentration is not well regulated and changes throughout the process, an error is introduced in the production rate estimation. In that case, the error equation for the residual biomass can be obtained from (6), (8), (12), (19) and (31):

$$\begin{aligned}
\dot{\tilde{x}} = \frac{\mu_{ps}x^2}{y_{ps}s} &- \frac{\hat{\mu}_{ps}\hat{x}^2}{y_{ps}s_r} - \left(\frac{x^2}{s} - \frac{\hat{x}^2}{s_r}\right)\frac{F_s s_f}{X} + \frac{V_m \dot{s}x^2}{Xs} \\
&+ \left(\bar{\rho}v\hat{x}^2\right)2\beta|\sigma|^{\frac{1}{2}}\mathrm{sign}(\sigma).
\end{aligned} \tag{43}$$

After convergence $x = \hat{x}$ and $\dot{\tilde{x}} = 0$, then it can be shown that:

$$\hat{\mu}_{ps} = \mu_{ps}\frac{s_r}{s} + \left(1 - \frac{s_r}{s}\right)\frac{F_s s_f y_{ps}}{X} + \frac{V_m \dot{s}y_{ps}}{X}\frac{s_r}{s}, \tag{44}$$

where it can be seen that the magnitude of the error depends mostly on how different the carbon source concentration is from the desired value $(\frac{s_r}{s})$ and how fast the carbon source changes.

Remark 3 Applying to (31) the map: $\left(\sigma(x,\hat{x}),\phi(\mu_{ps},\hat{\mu}_{ps})\right)$ with σ defined as in (31) and $\phi(\mu_{ps},\hat{\mu}_{ps}) = \frac{1}{\bar{\rho}}(\mu_{ps} - \hat{\mu}_{ps})$, the original super-twisting algorithm [9] can be obtained:

$$\begin{cases} \dot{\sigma} = \phi - 2\beta|\sigma|^{\frac{1}{2}}\text{sign}(\sigma) \\ \dot{\phi} = \dfrac{\dot{\hat{\mu}}_{ps}}{\bar{\rho}} - \alpha\,\text{sign}(\sigma) \end{cases}.$$

The stability of this system has been proven by a Lyapunov approach in [14].

Observer for the case with volume measurement

A different structure for the observer is proposed in this subsection for the scenario in which the volume is measured online. This case may be more appealing at an industrial level, since there is a wide variety of level sensors more frequently found in typical plants (capacitive, conductivity, radar, IR, laser, mechanical sensors). The stability analysis of the observer is similar to the previous case and will be omitted.

Based on Eq. (29), the proposed observer equations are:

$$\begin{cases} \dot{\hat{V}} &= F_s\gamma - \hat{\mu}_{ps}vX - (\bar{\rho}vX)2\beta|\sigma|^{\frac{1}{2}}\text{sign}(\sigma) \\ \dot{\hat{\mu}}_{ps} &= \bar{\rho}\alpha\,\text{sign}(\sigma) \\ \sigma &= (\bar{\rho}vX)^{-1}\left(V - \hat{V}\right), \end{cases} \tag{45}$$

where $\hat{V}$ and $\hat{\mu}_{ps}$ are the estimated volume and production rate, respectively, α and β are design gains, $\bar{\rho}$ is the bound for the production rate derivative and σ is the sliding function. As before, a map can be applied to obtain the original super-twisting algorithm: $\left(\sigma(V,\hat{V}),\phi(\mu_{ps},\hat{\mu}_{ps})\right)$ where $\phi(\mu_{ps},\hat{\mu}_{ps}) = \frac{\mu_{ps} - \hat{\mu}_{ps}}{\bar{\rho}}$.

Remark 4 This observer behaves similarly to the one in (31), particularly stability and finite time convergence still apply. The difference is that the information is taken from a volume measurement instead of the residual biomass concentration. This alternative can be advantageous in many cases, because the biomass sensors required for the measurement (capacitive probes) are very expensive and are not always available, especially in the industry where volume probes are very common.

Application example: PHB production

Polyhydroxybutyrate (PHB) is a bioplastic that can be obtained by fermentation using the bacteria *Cupriavidus necator* in a two-phase fed-batch reaction. It has been shown that PHB production by this bacteria has a strong non-growth-associated term and that nitrogen has a great inhibiting effect on it [16]. For this reason, in the first phase of the process, both nitrogen and carbon sources are fed to the microorganism to stimulate growth without PHB production. After reaching a large cell concentration, the nitrogen source is let to deplete completely while keeping the carbon source concentration at an optimal level. Nitrogen starvation conditions favor PHB production and at the same time halt cell proliferation; in this way, very high product to residual biomass ratios can be obtained [15]. In addition, there is evidence that cell volume increases linearly with PHB content [19].These process features make the proposed model and observer applicable to this problem.

The process model for the PHB production phase is as the one described in Eqs. (19)–(24), where x is the residual biomass concentration, p is the PHB concentration and s is the carbon source concentration (glucose in this example). The model is obtained from the one described in [15, 16] considering that there is no growth ($\mu_x = 0$) and feeding the carbon source at an adequate flow rate to keep its concentration nearly constant, and hence the production rate. In [16], a model for the PHB productions specific rate (μ_{ps}) is given, which in this work is used to simulate the process and to obtain the bound for $\dot{\mu}_{ps}$ ($|\dot{\mu}_{ps}| \leq \bar{\rho}$).

$$\mu_{\text{ps}} = \mu_{ps}^{\max} \cdot \frac{s}{k_s + s + \dfrac{s^2}{k_{\text{pis}}}} \cdot \left(1 - \left(\frac{f_{\text{phb}}}{f_{\text{phbm}}}\right)^{\eta}\right) \tag{46}$$

$$f_{\text{phb}} = \frac{p}{x}. \tag{47}$$

The variable f_{phb} is called PHB content ratio and will be later used in the experimental validation of the observer in Sect. 4.2.

In both the simulation results and experimental validation, the observer (31) is used. Similar results are obtained when using (45). Table 2 shows the values used in the observer parameters.

Simulation results

In this section, simulation results using the models described before are shown. Different process conditions are simulated and shown in Fig. 2a, b, c and d. In each case, the time evolution of the residual biomass x and its estimation $\hat{x}$ are shown in the top graph, the specific production rate μ_{ps} and its estimation $\hat{\mu}_{ps}$ in the middle graph, and the sliding function σ in the bottom graph. Except for Fig. 2b, real values of the variables (x and μ_{ps}) are plotted in dashed green lines and estimations in solid black lines. In all cases, the carbon source was regulated at 12 g/l, except for Fig. 2c where a bad regulation case is depicted.

The first simulation case is the observer response to initial conditions without external disturbances and is depicted in Fig. 2a. The initial conditions were

Table 2 Values of the parameters used in the simulations and experimental validation

| Name	Description	Value
y_{ps}	Carbon source to PHB yield	0.3 g/g
μ_{ps}^{max}	Maximum PHB production rate	$0.126\,\mathrm{h}^{-1}$
k_{ps}	Kinetic parameter	16.5 g/l
k_{pis}	Kinetic parameter	80 g/l
η	Kinetic parameter	7
f_{phbm}	Maximum PHB ratio	3.3 g /g
$V(0)$	Initial volume	0.897 l
$x(0)$	Initial residual biomass	47 g/l
F_s	Carbon source flow rate	18.6 ml/h
s_f	Carbon source concentration in the reservoir	650 g/l
s_r	Regulated carbon source concentration	12 g/l
ρ_p	Density of the product	1250 g/l
$\bar{\rho}$	Bound for $\dot{\mu}_{ps}$	0.026
v	Volume model parameter	-277 ml/g
γ	Volume model parameter	54.167
α	Gain of the proposed observer	5.5
β	Gain of the proposed observer	2.5

$\hat{x}(0) = 46\mathrm{g/l}$, $x(0) = 47\mathrm{g/l}$, $\hat{\mu}_{ps}(0) = 0\mathrm{h}^{-1}$, $\mu_{ps}(0) = 0.086\mathrm{h}^{-1}$. The most noticeable item is that both the residual biomass and production rate estimations converge in finite time to the real values (0.65 h, approximately), and small boxes are included in the graphics to further detail the convergence. As a consequence of the fact that no additional dynamics are added to the system, the observer keeps a perfect tracking after convergence and even while the production rate is dropping (real and estimated curves are overlapped when the tracking is good). The decay of the production rate is due to the PHB auto-inhibition [16]. Also, from the bottom graph, it can be observed that once the observer reaches the sliding surface ($\sigma = 0$) it never leaves it, which also illustrates the already mentioned tracking features. These are related to the fact that the production rate model is treated as a disturbance, which is completely rejected if the bound $\bar{\rho}$ is correct.

Figure 2b shows the observer response when low-frequency noise is added to the residual biomass measurement. The noise concentrates most of the power in the band between $2\,\mathrm{h}^{-1}$ and $10\,\mathrm{h}^{-1}$ (around 0.55 to 2.7×10^{-3} Hz), which results in variations of a few cycles per hour. The initial conditions were $\hat{x}(0) = 47\,\mathrm{g/l}$, $x(0) = 47\,\mathrm{g/l}$, $\hat{\mu}_{ps}(0) = 0\,\mathrm{h}^{-1}$, $\mu_{ps}(0) = 0.086\,\mathrm{h}^{-1}$. In the top graph, the solid green line is the residual biomass measurement and the dashed black line is the residual biomass estimation. In the middle graph, the solid green line is the production rate

estimation and the dashed black line is the real production rate. Although the measurement noise is inevitably present in the estimation, particularly due to its low frequency, the observer is still capable of tracking the real value under these conditions. The noise rejection capabilities of the observer are linked to the tuning of the gains α and β. In this case, the gains are set so the residual biomass estimation $\hat{x}$ does not follow the variations produced by noise, which are faster than the ones that are expected from the microorganism. If a smoother estimation is needed, filtering of the estimation or of the residual biomass measurement can be used. Another alternative is to add a dead zone to the $\mathrm{sign}(\sigma)$ function used in (31). Both alternatives gain smoothness of the production rate estimate, but lose tracking speed. Note that the noise in σ is expected from the fact that $\hat{x}$ is purposely smoother than x, and the amplitude increase at the end of the process is simply because the noise amplitude remained constant while residual biomass decreased significantly.

Figure 2c shows a case where carbon source concentration s (blue dashed–dotted line in the top graph) is fluctuating instead of being regulated at a constant value, resulting in a variation on the production rate and a mismatch between the real γ and v parameters and the ones used in the observer. The profile used to simulate the variation is similar to many found in experimental cases, but exaggerated to test the observer; see [15] for instance. The initial conditions used are $\hat{x}(0) = 47\,\mathrm{g/l}$, $x(0) = 47\,\mathrm{g/l}$, $\hat{\mu}_{ps}(0) = 0\,\mathrm{h}^{-1}$, $\mu_{ps}(0) = 0.089\,\mathrm{h}^{-1}$. It can be seen that although the glucose concentration has a different value than the expected one, the error introduced in the estimation is small, particularly for monitoring or extremum-seeking control purposes. The magnitude of the error in the production rate estimation is described in (44).

Finally, Fig. 2d depicts a case with sensor failures, to show how the sliding function σ is useful to detect such events. The estimation made by an exponential observer ($\hat{\mu}_{ps-\exp}$) is additionally shown in blue dashed–dotted line to compare with the one made by the proposed HOSM observer ($\hat{\mu}_{ps-\mathrm{hosm}}$). The initial conditions used are $\hat{x}(0) = 47\,\mathrm{g/l}$, $x(0) = 47\,\mathrm{g/l}$, $\hat{\mu}_{ps-\mathrm{hosm}}(0) = \hat{\mu}_{ps-\exp}(0) = 0\,\mathrm{h}^{-1}$, $\mu_{ps}(0) = 0.086\,\mathrm{h}^{-1}$. Between 10 and 20 h, a constant offset of 10 g/l appears in the residual biomass measurement x_m. From the top graph, it can be seen that both observers track the measured biomass with similar speeds, with the exponential observer estimation having some overshoot (see small box). The production rate estimations show similar perturbations when the offset starts and finishes; however, these are shorter in time in the case of the HOSM observer. Also, some constant error is produced in
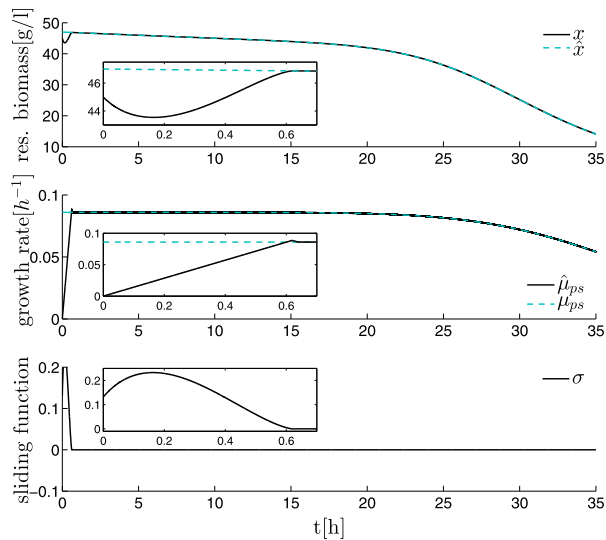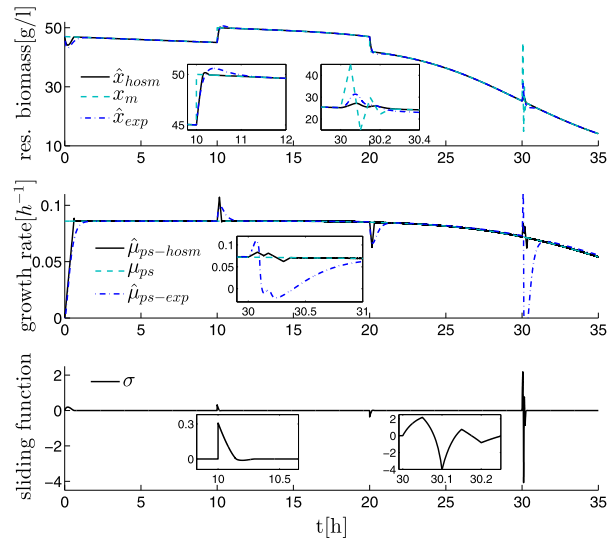
(a) Observer response to initial conditions (without disturbances). $\hat{x}(0) = 45g/l$, $x(0) = 47g/l$, $\hat{\mu}_{ps}(0) = 0h^{-1}$, $\mu_{ps}(0) = 0.086h^{-1}$
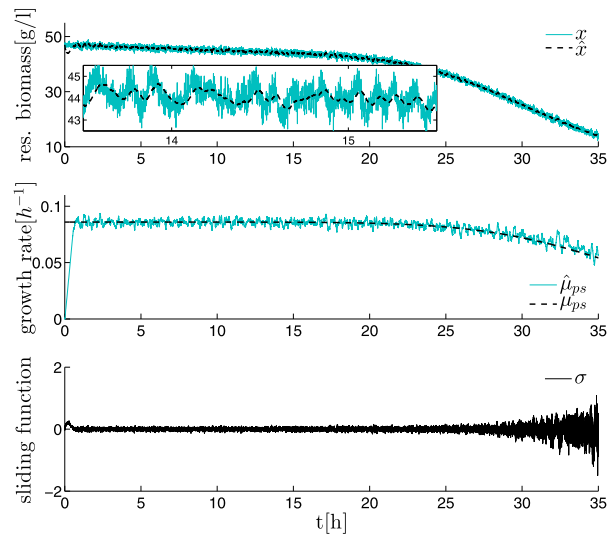
(b) Observer response under low frequency noise. $\hat{x}(0) = 47g/l$, $x(0) = 47g/l$, $\hat{\mu}_{ps}(0) = 0h^{-1}$, $\mu_{ps}(0) = 0.086h^{-1}$
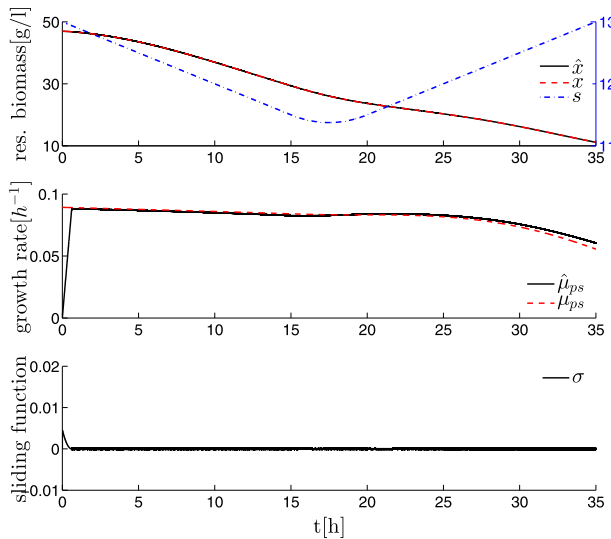
(c) Observer response under bad glucose regulation. $\hat{x}(0) = 47g/l$, $x(0) = 47g/l$, $\hat{\mu}_{ps}(0) = 0h^{-1}$, $\mu_{ps}(0) = 0.089h^{-1}$

(d) Observer response under sensor failures. $\hat{x}(0) = 47g/l$, $x(0) = 47g/l$, $\hat{\mu}_{ps-hosm}(0) = \hat{\mu}_{ps-exp}(0) = 0h^{-1}$, $\mu_{ps}(0) = 0.086h^{-1}$

Fig. 2 Simulation results: *top* graph, biomass. *Middle* graph, specific production rate. *Bottom* graph, commutation function

the estimation while the offset exists; nevertheless, it is too small to be noticed. At time 30 h, some spikes appear in the biomass measurement x_m with a peak of 20 g/l. The spikes have a fast slew rate and could be caused by a sensor malfunction or disconnection. In the case of the residual biomass estimations, both observers present a smooth oscillation; however, the HOSM observer estimation is more damped. A stronger difference is seen in the

production rate estimation, while the exponential observer produces a $\hat{\mu}_{ps-exp}$ estimate with an excessively large overshoot and slow response (see small box), the HOSM observer produces an estimation $\hat{\mu}_{ps-hosm}$ significantly more damped and with faster convergence. While the offset perturbation affects equally both observers, the perturbation introduced by the spikes is much better rejected by the HOSM observer. Last but not least, the sliding function in

the bottom graph can be used as a coordinate to detect these kinds of failures. Each time one of the events happens, σ escapes the surface ($\sigma \neq 0$) and shows spikes as in $t = 10$h, $t = 20$h and $t = 30$h. The magnitude of the spikes is not only an indicator of the failures, but also its duration in time. By monitoring σ, these abnormal effects can be detected.

Experimental validation

In this section, experimental results are shown for the observer when used with data measured in a real process. In our experiments, the only variables measured online are the carbon source flow rate and alkali solution flow rate (for pH control) with a sample time of 1 min. The residual biomass concentration was measured offline by taking samples every couple hours (the period was between 1 and 5 h). To test the observer, a continuous residual biomass measurement is needed, at least with a sampling time of a few minutes. Since this kind of measurement was not available, to obtain a continuous residual biomass signal, the off-line samples were interpolated with first-order polynomials and sampled with the same sampling time as the flow rates. The observer algorithm was run with a frequency of 1 Hz. The fed-carbon source was glucose at 650 g/l, and the concentration in the bioreactor was regulated at a value of 12 g/l. Each time a sample is taken from the bioreactor, the total biomass weight decreases. This fact is taken into account by adapting the X value at the corresponding time instant.

Figure 3 shows the results for two different experiments. Figure 3a, c correspond to experiment **A** and Fig. 3b, d correspond to experiment **B**. Figure 3a, b show the observer variables for each experiment. In the top graph, the time evolution of the residual biomass x (interpolated samples) and its estimation $\hat{x}$ is plotted in dashed green and solid black line, respectively. The middle graph shows the specific production rate estimation $\hat{\mu}_{ps}$ in solid black line and two reference values for μ_{ps}. The dashed green line is the production rate constant value $\mu_{set-point}$ expected from the feeding profile used in [15]. The red squares are another reference obtained by differentiating the PHB to biomass ratio $f_{phb} = \frac{p}{x}$ (47) which is equivalent to the production rate μ_{ps}; see "Appendix". Note however, that the later should not be considered as the real value or as good as a direct measurement, since the differentiation amplifies noise and is sensitive to measurement errors; moreover, it is calculated over a few samples. The bottom graph shows the commutation function σ; the noise in this variable is due to the discretization of the algorithm and it can be reduced

by simply increasing the frequency of execution. Both experiments give good residual biomass estimations and production rate estimations close to the references, and also the sliding function σ stays in the surface all the time.

To further verify the goodness of the production rate estimation, two open-loop[2] estimations are shown Fig. 3c, d. In the top graph the PHB content ratio f_{PHB} is compared to the integral of the estimated production rate ("Appendix"). The green squares are the PHB content ratio calculated from the off-line samples as $f_{phb} = \frac{p}{x}$ and the black solid line is the integral of the estimated production rate. To avoid the error introduced by integrating the initial transient of the production rate estimation, the integral was restarted at the convergence time (5th h). In the bottom graph, the bioreactor volume is compared to the volume estimation by integration of the model given in (14) using the estimated production rate. The bioreactor volume is calculated from the off-line samples as $\frac{X}{x}$ and is represented with green circles. The solid black line is the volume estimation obtained by replacing $\hat{\mu}_{ps}$ in Eq. (14) and integrating it. Again, to avoid the error introduced by the initial transient of $\hat{\mu}_{ps}$, the integral was restarted at the convergence time. As can be seen, the fitting between the estimations and real values is very good for both experiments.

Discussion

The experimental results show that the proposed volume model (17) makes good volume predictions as it can be seen in Fig. 3c, d. The improved performance of this model is due to the addition of the terms accounting for the product volume and carbon source consumption. Uncertainty in the model parameters γ and ν (see 15 and 16) can show up if the carbon source concentration is different from the desired value. However, if the concentration in the bioreactor is not excessively different from the desired one, the error in the parameters will be small and will not affect the model predictions significantly.

With regard to the proposed observer, the simulations allowed to verify its performance under different scenarios. For a start, the observer is able to track the production rate of the process without the use of a kinetic model. Finite time convergence is achieved in all cases, including the experimental validation, which can be noticed when σ reaches the surface. After convergence, no delays or dynamics are added to the estimation; that means, it

---

[2] These are called open-loop because there is no feedback or correction term applied to the calculation, and, there is no convergence guarantee.
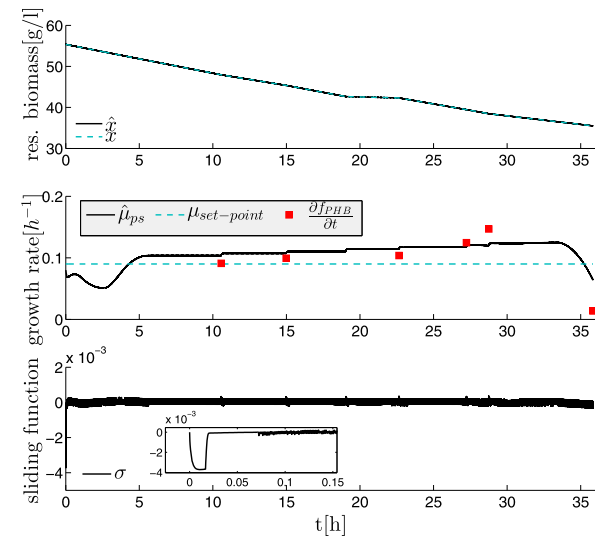
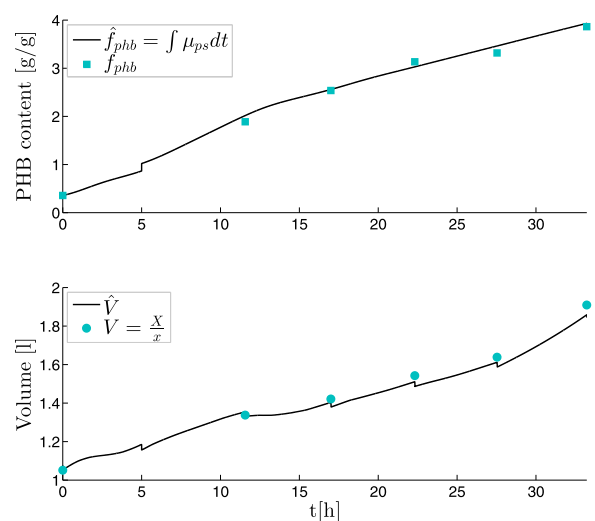**(a)** Experiment **A**: Top graph, residual biomass. Middle graph, specific production rate. Bottom graph, commutation function. $\hat{x}(0) = x(0) = 55.3g/l, \hat{\mu}_{ps}(0) = 0.09h^{-1}$
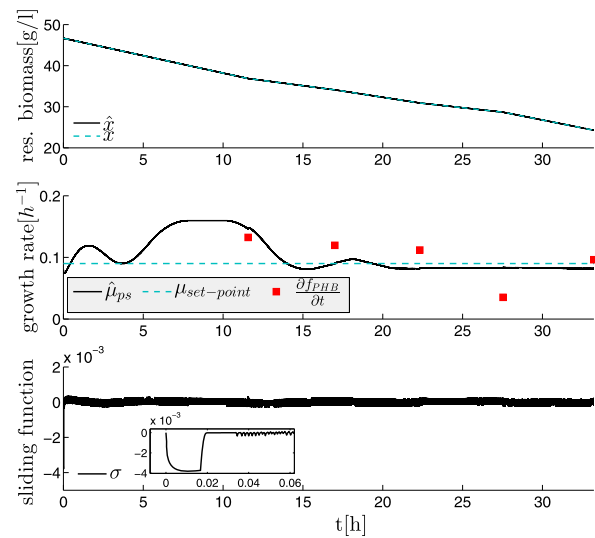
(b) Experiment **B**: Top graph, residual biomass. Middle graph, specific production rate. Bottom graph, commutation function. $\hat{x}(0) = x(0) = 46.7g/l, \hat{\mu}_{ps}(0) = 0.09h^{-1}$
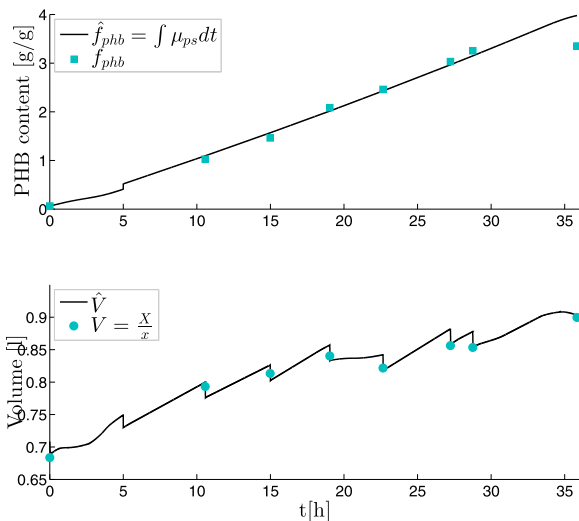
(c) Experiment **A**: Top graph, intracellular PHB content. Bottom graph, volume. $V(0) = 0.7l$

(d) Experiment **B**: Top graph, intracellular PHB content. Bottom graph, volume. $V(0) = 1.1l$

Fig. 3 Experimental results

perfectly tracks the production rate. The carbon source concentration variations and γ and ν uncertainty had little effect on the estimation (Fig. 2c). In fact, the stability of the observer is not compromised, and the estimation errors converge to a neighborhood of zero with bound given by (44). The effect of noise is also small on the estimation; while differentiation would have heavily amplified the noise in the residual biomass measurement, the observer is able to keep track of the rate showing only a small level of noise which can be suppressed with a low-pass filter.

Conclusions

In this work, a new model was obtained to describe volume changes in high cell density fed-batch processes with intracellular product accumulation. High-order sliding mode observers were developed to estimate the production rate in those processes, and stability proofs for the errors were given. Both the volume and the observer were tested in simulation and validated experimentally.

The proposed model is an improved description of the volume changes in high cell density processes, as shown by

the experimental results. The model served as the basis for design of the HOSM observer. The observer results also showed a good performance under noise and substrate changes. The fast and finite time convergence is an advantage for its application in bioprocesses. The algorithm is simple enough to be implemented in standard laboratory or industrial equipment. It has the alternative to use either a biomass sensor or a level sensor, which may be of interest for industrial applications.

The results obtained in this work, together to the ones obtained for growth rate estimation [8], open the possibility to start working in the closed-loop control of PHB processes. The estimated rates can be used to maximize the productivities with extremum-seeking control.

Appendix: Useful formulas

Given a process described by:

$$\dot{x} = -Dx \tag{48}$$

$$\dot{p} = \mu_{ps}x - Dp, \tag{49}$$

It follows that:

$$\int_0^t \mu_{ps} = \frac{p(t)}{x(t)} - \frac{p(0)}{x(0)}. \tag{50}$$

Proof

$$\frac{\partial}{\partial t}\left(\frac{p}{x}\right) = \frac{\dot{p}x - p\dot{x}}{x^2}$$

$$= \frac{\left(\mu_{ps}x - Dp\right)x + Dxp}{x^2} = \frac{\mu_{ps}x^2}{x^2} = \mu_{ps}$$

Then by integration (50) is obtained. □

References

1. Boyd S, El Ghaoui L, Feron E, Balakrishnan V (1994) Linear Matrix Inequalities in System and Control Theory, Studies in Applied Mathematics, vol 15. SIAM, Philadelphia

2. Chang DM (2003) The snowball effect in fed-batch bioreactions. Biotechnol Progress 19(3):1064–1070

3. De Battista H, Picó J, Picó-Marco E (2006) Globally stabilizing control of fed-batch processes with Haldane kinetics using growth rate estimation feedback. J Process Control 16(8):865–875

4. De Battista H, Picó J, Garelli F, Navarro JL (2012a) Reaction rate reconstruction from biomass concentration measurement in bioreactors using modified second-order sliding mode algorithms. Bioprocess Biosyst Eng 35(9):1615–1625

5. De Battista H, Picó J, Picó-Marco E (2012b) Nonlinear PI control of fed-batch processes for growth rate regulation. J Process Control 22(4):789–797

6. Dochain D (2003) State and parameter estimation in chemical and biochemical processes: a tutorial. J Process Control 13(8):801–818

7. Ehgartner D, Sagmeister P, Herwig C, Wechselberger P (2015) A novel real-time method to estimate volumetric mass biodensity based on the combination of dielectric spectroscopy and soft-sensors. J Chem Technol Biotechnol 90(July):262–272

8. Jamilis M, Garelli F, Mozumder MSI, Volcke E, De Battista H (2015) Specific growth rate observer for the growing phase of a polyhydroxybutyrate production process. Bioprocess Biosyst Eng 38(3):557–567

9. Levant A (1998) Robust exact differentiation via sliding mode technique. Automatica 34(3):379–384

10. Li L, Wang ZJ, Chen XJ, Chu J, Zhuang YP, Zhang SL (2014) Optimization of polyhydroxyalkanoates fermentations with on-line capacitance measurement. Bioresource Technol 156:216–221

11. Li Y, Zhao ZK, Bai F (2007) High-density cultivation of oleaginous yeast Rhodosporidium toruloides Y4 in fed-batch culture. Enzyme Microbial Technol 41(3):312–317

12. Löfberg J (2004) Yalmip: A toolbox for modeling and optimization in MATLAB. In: Proceedings of the CACSD Conference, Taipei, Taiwan. URL http://users.isy.liu.se/johanl/yalmip

13. Maskow T, Röllich A, Fetzer I, Yao J, Harms H (2008) Observation of non-linear biomass-capacitance correlations: reasons and implications for bioprocess control. Biosens Bioelectron 24(1):123–128

14. Moreno J, Osorio M (2008) A Lyapunov approach to second-order sliding mode controllers and observers. In: 47th IEEE Conference on Decision and Control. pp 2856–2861

15. Mozumder MSI, De Wever H, Volcke EI, Garcia-Gonzalez L (2014a) A robust fed-batch feeding strategy independent of the carbon source for optimal polyhydroxybutyrate production. Process Biochem 49(3):365–373

16. Mozumder MSI, Goormachtigh L, Garcia-Gonzalez L, De Wever H, Volcke EIP (2014b) Modeling pure culture heterotrophic production of polyhydroxybutyrate (PHB). Bioresource Technol 155:272–280

17. Nuñez S, De Battista H, Garelli F, Vignoni A, Picó J (2013) Second-order sliding mode observer for multiple kinetic rates estimation in bioprocesses. Control Eng Practice 21(9):1259–1265

18. Papanikolaou S, Aggelis G (2011) Lipids of oleaginous yeasts. part ii: Technology and potential applications. Eur J Lipid Sci Technol 113(8):1052–1073

19. Pedrós-Alió C, Mas J, Guerrero R (1985) The influence of poly-β-hydroxybutyrate accumulation on cell volume and buoyant density in Alcaligenes eutrophus. Archives of microbiology. pp 178–184

20. Picó J, De Battista H, Garelli F (2009) Smooth sliding-mode observers for specific growth rate and substrate from biomass measurement. J Process Control 19(8):1314–1323

21. Reddy CSK, Ghai R, Rashmi Kalia VC (2003) Polyhydroxyalkanoates: an overview. Bioresource Technol 87(2):137–146

22. Riesenberg D, Guthke R (1999) High-cell-density cultivation of microorganisms. Appl Microbiol Biotechnol 51(4):422–430

23. Sagmeister P, Wechselberger P, Jazini M, Meitz A, Langemann T, Herwig C (2013) Soft sensor assisted dynamic bioprocess control: efficient tools for bioprocess development. Chem Eng Sci 96:190–198

24. Suzuki T, Mori H, Yamané T, Shimizu S (1985) Automatic supplementation of minerals in fed-batch culture to high cell mass concentration. Biotechnol Bioeng 27:192–201

25. Vargas A, Moreno J, Wouwer AV (2014) A weighted variable gain super-twisting observer for the estimation of kinetic rates in biological systems. J Process Control 24(6):957–965 **(energy Efficient Buildings Special Issue)**

26. Yang X, Jin G, Gong Z, Shen H, Bai F, Zhao ZK (2014) Recycling biodiesel-derived glycerol by the oleaginous yeast Rhodosporidium toruloides Y4 through the two-stage lipid production process. Biochem Eng J 91:86–91